Aust. J. Phys., 1974, **27**, 687–711

An Aperture Synthesis Survey of the Galactic Plane

B. B. Jones[A,B] *and E. A. Finlay*[A]

[A] School of Electrical Engineering, University of Sydney, Sydney, N.S.W. 2006.
[B] Present address: Max-Planck Institut für Radioastronomie, 53 Bonn 1, Auf dem Hügel 69, West Germany.

Abstract

The results of a survey already published have been used to construct contour maps and ruled surface diagrams of the brightness temperature at 29·9 MHz near the galactic plane between $l = 225°$ and 30°. The angular resolution was 0°·8 at the zenith, and the range of zenith angles involved was ±30°. Restoration of the background was achieved with the aid of a low resolution filled-aperture survey carried out by others. The brightness temperature scale was calibrated absolutely. The optical depth of the Galaxy in directions within 40° of latitude from the centre has been estimated by a method which relies only on the shapes of brightness temperature profiles and not on absolute temperature calibrations. If an electron temperature is assumed, r.m.s. electron densities can be deduced. The average value of the disc emissivity at 29·9 MHz and the value of its spectral index have been calculated from brightness temperature profiles observed at a number of different frequencies, calibrations being required for these purposes. About 29 discrete absorption regions have been observed and identified with optically observed HII regions, and the fact that these are all nearer than 4 kpc permits a choice between kinematic distances in two cases. The Carina nebula and RCW 108 lend themselves to the measurement of local emissivities, and values of these together with their implications have already been published. A number of previously unlisted nonthermal sources have been observed, many of which are objects of low surface brightness and probably are supernova remnants.

1. Introduction

The survey of the galactic plane presented here forms part of a survey covering the region of sky between declinations −4° and −64° which has been carried out at Fleurs, N.S.W. The frequency of 29·9 MHz used for the survey is well suited for observing details of the absorption of galactic radiation by thermal electrons. At frequencies below about 50 MHz the brightness temperature of the distributed radiation from the Galaxy is nearly everywhere higher than the electron temperatures of the ionized gas clouds of the Galaxy, and at 30 MHz even the brightness temperature of the isotropic extragalactic radiation is probably greater than the electron temperatures of the ionized gas. These clouds absorb the low frequency radiation passing through them and so appear as depressions in brightness whereas at higher frequencies they appear as sources. In particular, the absorption of radiation from the disc of the Galaxy by ionized interstellar gas can be examined at 30 MHz because at this frequency the absorption is significant, but still the transmission of radiation from the inner portions of the Galaxy is substantial. The absorption of radiation from the inner arms of the Galaxy at frequencies below about 15 MHz is almost complete, and so observations at these frequencies can only provide information on conditions within a few kiloparsecs of the Sun and not on conditions representative of the whole of the disc. Measurement of the absorption coefficient of the interstellar medium

provides information which supplements high frequency radio recombination line and continuum results in testing models of the interstellar medium.

The aerial used for the 29·9 MHz survey consisted of an east–west (EW) array of 212 collinear half-wave elements which gave a fan beam along the meridian. This array was used in conjunction with two movable arrays each consisting of three half-wave dipoles fed in phase. These two movable aerials were placed symmetrically to the north and south of the EW array at a number of spacings in order to obtain resolution in the north–south (NS) direction using aperture synthesis. After observations had been made with the north and south aerials in each of 50 positions, maps of sky brightness were obtained by Fourier transformation. A description of the telescope and of most of the observing procedures and methods of computation have already been published (Finlay and Jones 1972, 1973; Jones 1973). The half-power width of the synthesized beam was 0°·8 in right ascension and $0°\cdot8\sec(\delta+33°\cdot86)$ in declination at declination δ, the latitude of the Fleurs observatory being 33°·86S.

2. Brightness Temperature Observations

(*a*) *Temperature Scale*

Maps of brightness temperature were drawn by computer using an essentially arbitrary contour unit which arose from the calibration techniques employed during the observations. The interval of brightness temperature corresponding to the contour unit was determined from the observed responses to a number of point sources using the fact that in the absence of polarization a region of brightness temperature T_b produces a response equal to the peak response due to a source of strength S if

$$T_b = \lambda^2 S/\{2k\Omega_m \sec(\delta+33°\cdot86)\},$$

where λ is the wavelength, k Boltzmann's constant and Ω_m the main lobe solid angle of the synthesized beam at the zenith. Values of S for the sources used were based on a flux density of 1510 Jy* for Hydra A (Finlay and Jones 1973). The value obtained for Ω_m from the response on the maps to point sources was $2\cdot60\times10^{-4}$ sr, which agreed with the value expected from the gradings of the EW array and the NS array of spacings to within 1%. These values of S and Ω_m gave a temperature scale of 1 contour unit = 1470 K.

(*b*) *Restoration of Background*

As with all surveys carried out with an interferometer-type instrument, it was not possible to measure the lowest spatial frequency components of the sky brightness directly because of interaction between aerials. In the closest position, the N and S aerials were spaced $0\cdot38\lambda$ from the centre line of the EW array. They could not occupy these positions simultaneously without overlapping physically, so they were placed in position one at a time and the resulting outputs were combined numerically. Thus the question of interaction between the N and S aerials did not arise. However, it was clear that severe interaction was occurring between the EW array and the N and S aerials, and to eliminate this a section of the EW array 2λ in extent was removed. The composite $0\cdot38\lambda$ records were then deficient by an amount equal to the outputs which a hypothetical interferometer consisting of the N and S aerials and the missing

* 1 jansky (Jy) = 10^{-26} W m^{-2} Hz^{-1}.

2λ portion of the EW array would have produced in the absence of interaction between its elements.

A correction for this deficiency was calculated from the low resolution survey of the southern sky made at 30 MHz with the Parkes dish (Mathewson *et al.* 1965). In order to do this, it was necessary to calculate the beam shapes of the N or S aerial and of the missing portion of the EW array, and to measure the ohmic efficiency of the EW array. Only the shape of the brightness distribution found by Mathewson *et al.* was utilized; an absolute calibration was obtained by measuring the aerial temperature of the N aerial between 04^h and 05^h sidereal time, when the brightness temperature of the sky is fairly constant. Several factors, however, limit the accuracy of this assessment of the missing component. The most serious of these is the fact that the Parkes survey does not extend north of the equator and the beam of the interferometer being simulated does have a small part of the main beam and a sidelobe in this region. Its temperature was assumed constant and equal to the average temperature seen by the rest of the beam, leading to some error in the background levels, particularly when the galactic plane crosses the meridian at a large zenith angle.

The second closest spacing of the N and S aerials was such that their centre lines were distant $1{\cdot}13\lambda$ from the centre line of the EW array, and it was assumed that interaction between aerials was not serious at this and larger spacings.

The synthesized maps do not show marked periodicities in the NS direction corresponding to a spacing of $0{\cdot}38\lambda$ and the temperatures of uniform temperature regions of the synthesized maps agree fairly well with those of the Parkes maps. On this basis it is thought that the background level of the synthesized maps is accurate to about ± 2000 K except in the part of the sky near the galactic centre, where the error may reach 20 000 K. Thus the background level is accurate to about two contour intervals in each section of the map. Temperature differences between points closer together than about 30° are of course much more accurate.

Inaccuracies also occur in the observed temperatures due to uncertainty in the flux of the reference source, Hydra A (estimated to be 10%), and to random noise. The r.m.s. noise level depends on the aerial temperatures and ranges from about 3 contour units at 18^h right ascension to about 0·6 contour units at 08^h.

(*c*) *Ruled Surface Diagrams*

Before the contour maps were drawn, sets of values of sky brightness for each minute of right ascension were calculated and stored, and from these data graphs of brightness versus declination were drawn using the plotter. The graphs for successive minutes of right ascension were displaced at right angles to the declination axis, giving the pictures a three-dimensional appearance. The first profiles produced in this way (Finlay and Jones 1972) showed ripples along lines of constant declination, particularly at the zenith, which were due to signal from the NS aerials leaking into the EW receiver and producing offsets. The magnitude of these ripples reached a maximum corresponding to about 5000 K near the centre of the Galaxy. Since the spurious output was proportional to the temperature T_{NS} of the NS aerials, the ripples were removed by fitting a quantity $aT_{NS}+b$ to the interferometer records, with regions around strong sources removed, and then subtracting this quantity from the records.

The sets of ruled surface diagrams which show the galactic plane most clearly are those of Figs 1*a*, 1*b* and 1*c*. The plane is clearly evident from about right ascension

16^h to 19^h, at which latter value it passes outside the surveyed region. Over most of this range of right ascension it appears as a complex succession of troughs.

The very large peak at declination $-28°$ in Fig. 1*b* lies on the galactic plane, a little to the west of the galactic centre. There is a marked hollow very close to the centre but it is obscured by the large peak at declination $-30°$. The strong unresolved source near the left-hand edge of Fig. 1*a* (1610−61) gives an impression of the size of the synthesized beam and of the grating lobes which are produced by a source located near the boundary of the surveyed region.

(*d*) *Contour Maps*

The contour maps of Fig. 2* show the distribution of brightness temperature near the galactic plane between longitudes $l = 225°$ and $30°$. The contour interval is related to brightness by 1 contour unit = 1470 K (see subsection *a* above). The strip between right ascensions $13^h\,15^m$ and $13^h\,30^m$ (Fig. 2*d*) was seriously affected by ripples due to Centaurus A and has been omitted. Similarly, spurious features due to Virgo A may appear in the vicinity of right ascension $12^h\,28^m$.

Because of the variation of beamwidth over each map, the flux density scale is not uniform. A source with peak beam temperature of one contour unit at declination δ has a flux density of $10{\cdot}4\sec(\delta+33°{\cdot}86)$ Jy, based on a flux density of 1510 Jy for Hydra A. The contour interval has been changed in several places because of the large range of brightness over the region mapped: In Fig. 2*b* the contour interval is increased from one to two contour units around the Vela–Puppis complex in the region $08^h\,15^m<\alpha<09^h\,00^m$ and $-40°>\delta>-50°$. In Fig. 2*d* the contour interval is increased from one to two units for $\alpha>12^h\,00^m$ and in Figs 2*e* and 2*f* the contour interval is 10 units (14 700 K).

3. Analysis of Results

(*a*) *Disc Absorption*

Comparison at low and high frequencies of brightness profiles across the galactic plane at longitudes which are free of HII regions can give information about the spectrum of the nonthermal disc radiation and about the optical depth of the Galaxy along paths passing close to the galactic centre. It is not really satisfactory to compare the temperatures given in Figs 2*e* and 2*f*, however, with those given in high frequency galactic surveys because of the uncertainty in the restoration of the $0{\cdot}38\,\lambda$ spacing component in this region. It is better to compare the shapes of the profiles without making use of absolute levels. The method adopted makes use of the fact that the nonthermal emitting region appears to be nearly disc-shaped from the observation that over a range of latitudes the brightness temperature distribution resulting from nonthermal emission is given by

$$T_b = A\,\mathrm{cosec}\,b + B, \qquad (1)$$

in which A and B are functions of frequency and b is the galactic latitude. This relation is followed over the range $1°{\cdot}3<|b|<20°$. The upper limit of latitude is apparent in Fig. 3*a*, and the lower limit in Fig. 3*b*, in both of which T_b is plotted against $\mathrm{cosec}\,b$ (see p. 700). Fig. 3*a*, which has been taken from Baldwin (1968), shows the results of 400 MHz observations, while Fig. 3*b* has been derived from the 1410 MHz maps of Altenhoff *et al.* (1970).

* Larger versions of these maps are available from the author on request.

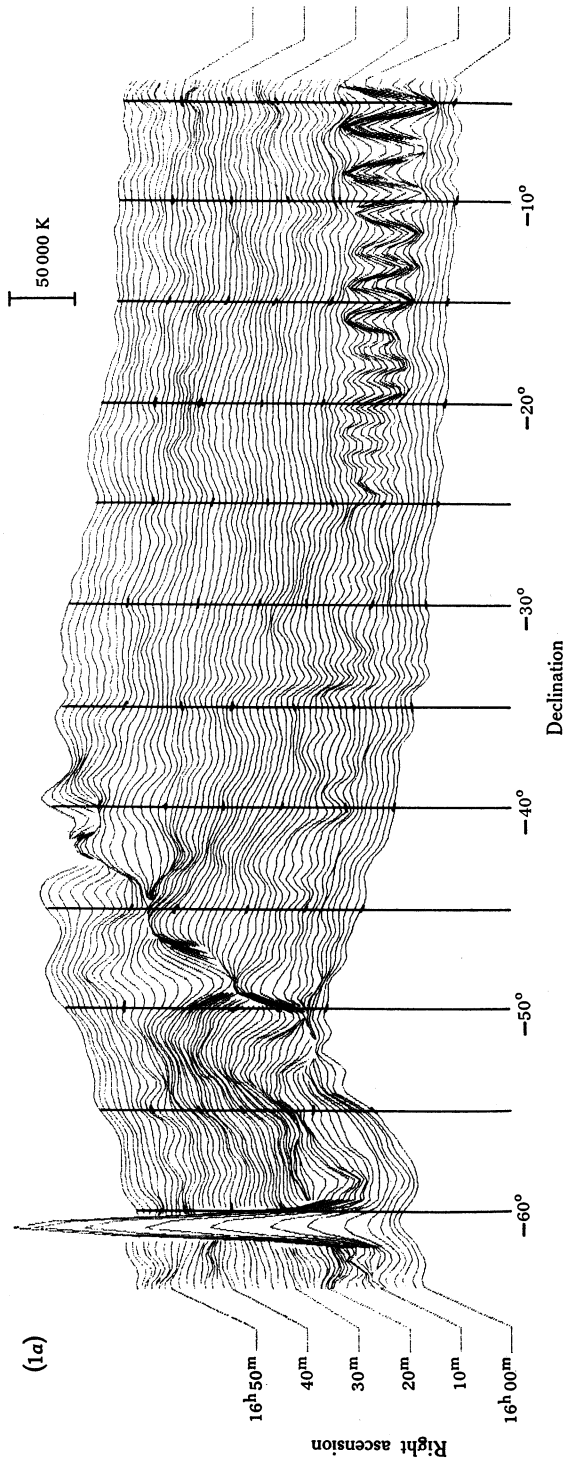

Figs 1a–1c. Ruled surface diagrams showing brightness profiles in which the galactic plane is clearly evident.

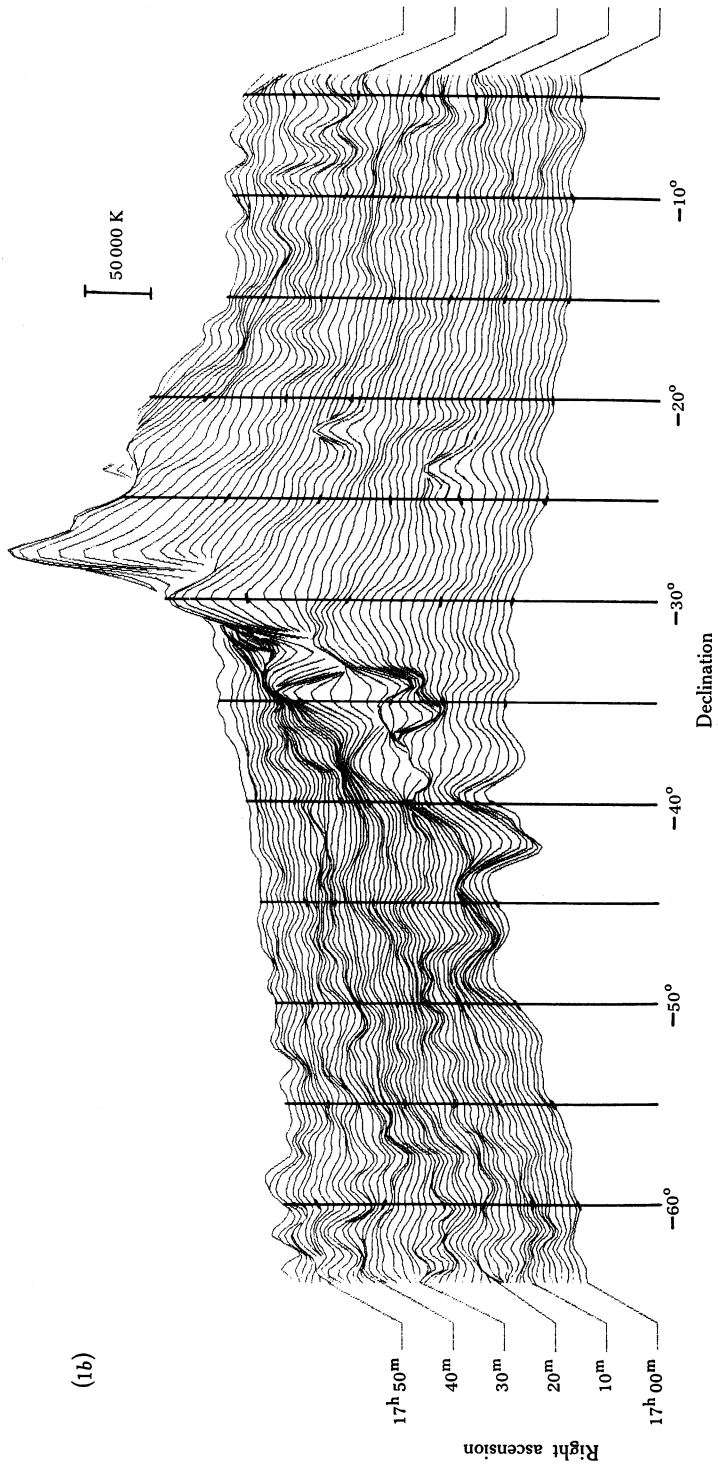
50 000 K
−10°
−20°
−30°
−40°
−50°
−60°
Declination
17h 50m
40m
30m
20m
10m
17h 00m
Right ascension

(1b)

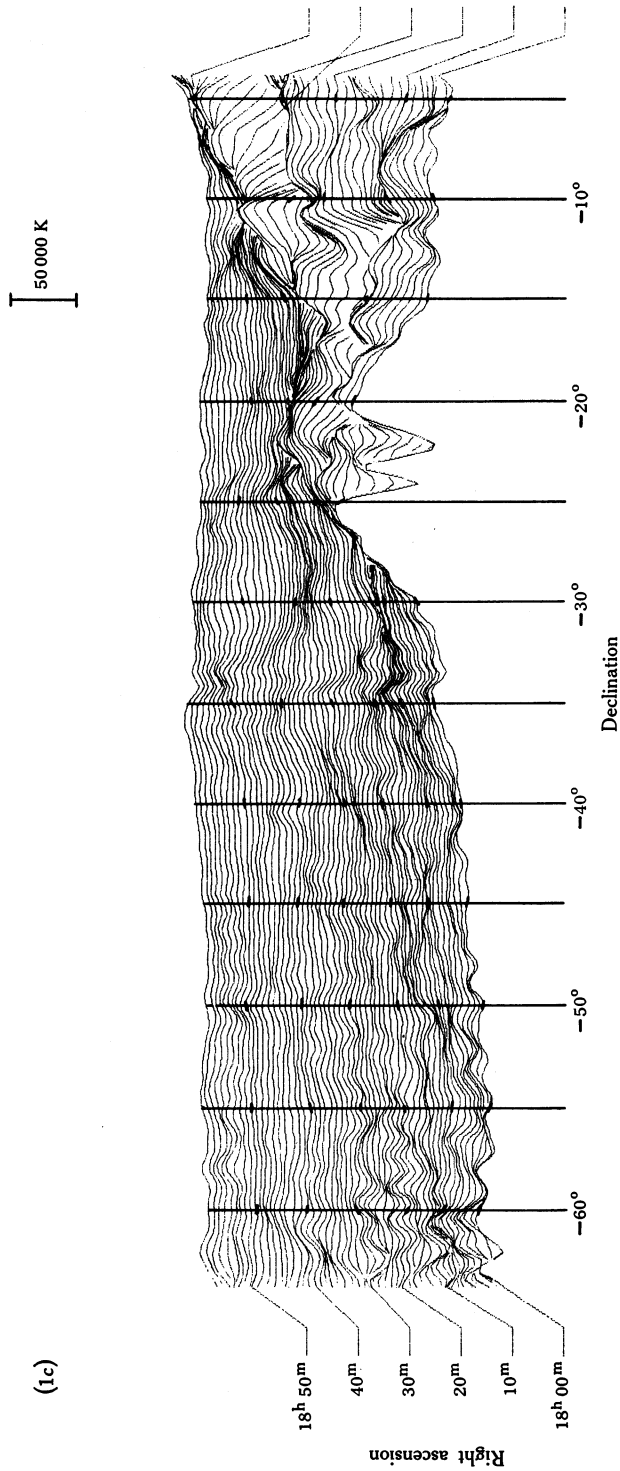
50 000 K
−10°
−20°
−30°
−40°
−50°
−60°
Declination
18h 50m
40m
30m
20m
10m
18h 00m
Right ascension
(1c)

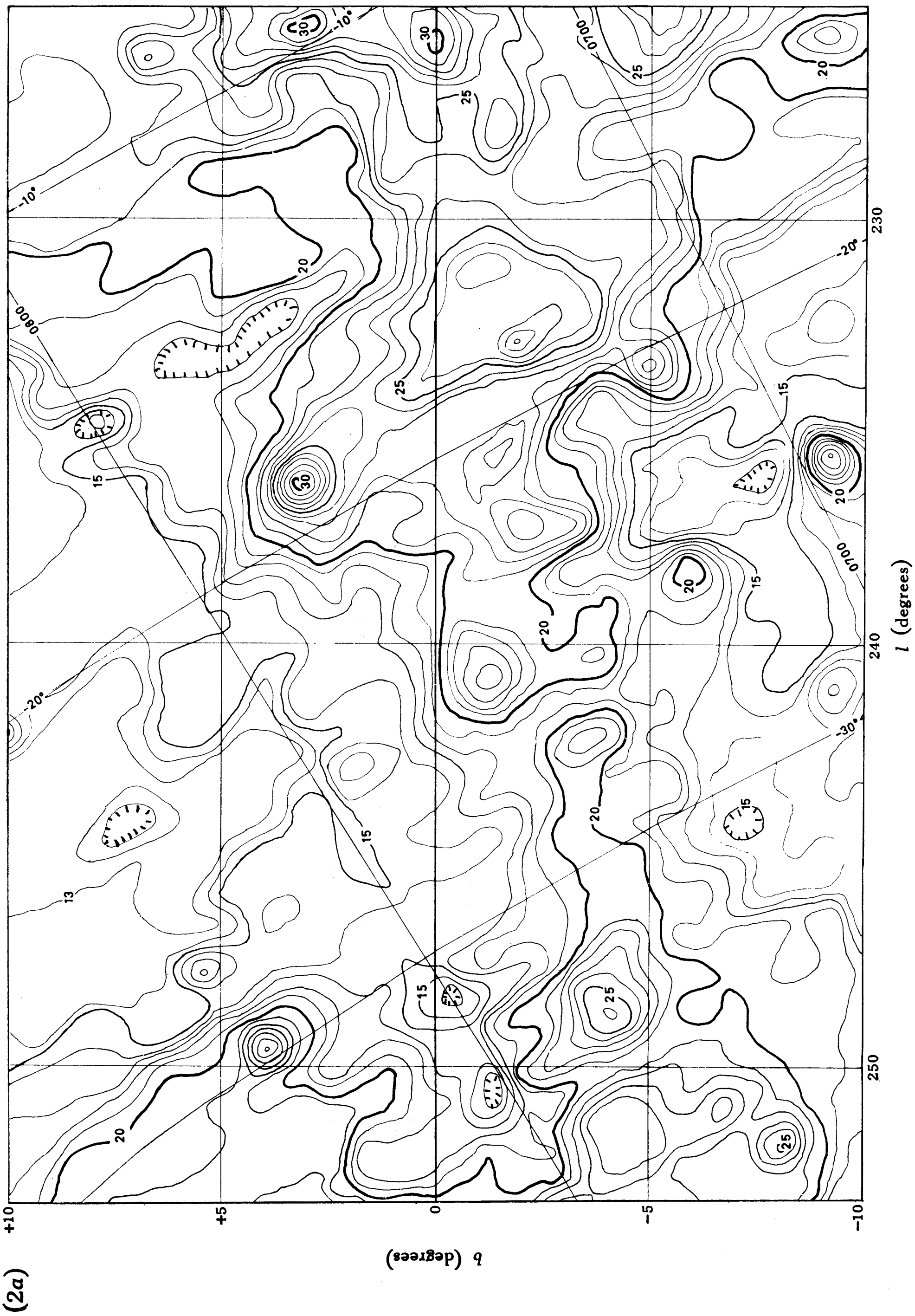

(2a)

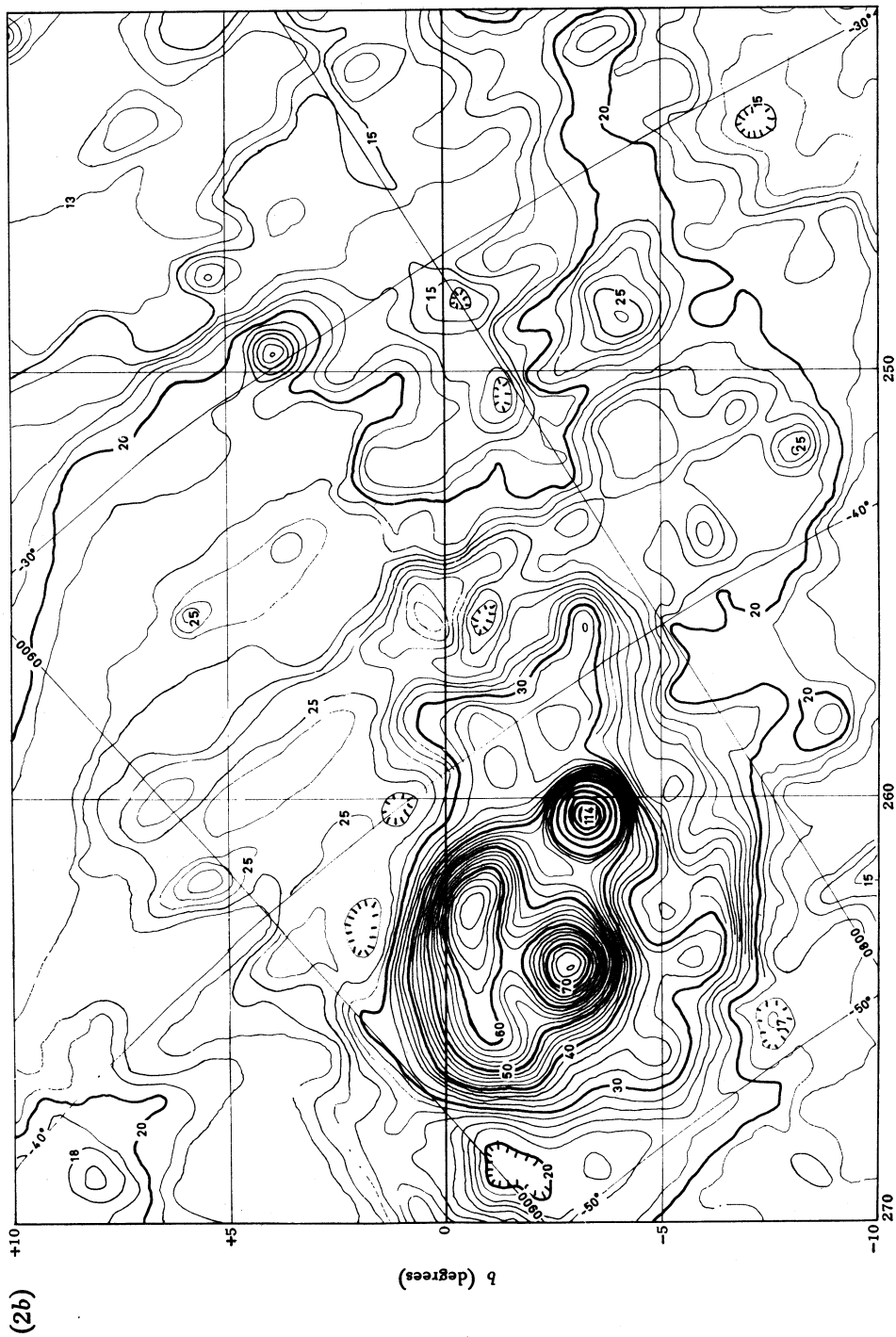
(2b)
b (degrees)
+10
+5
0
-5
-10
l (degrees)
270
260
250
-30°
-40°
-50°
-60°
-70°
-80°
-90°
15
20
25
30
50
60
70
114

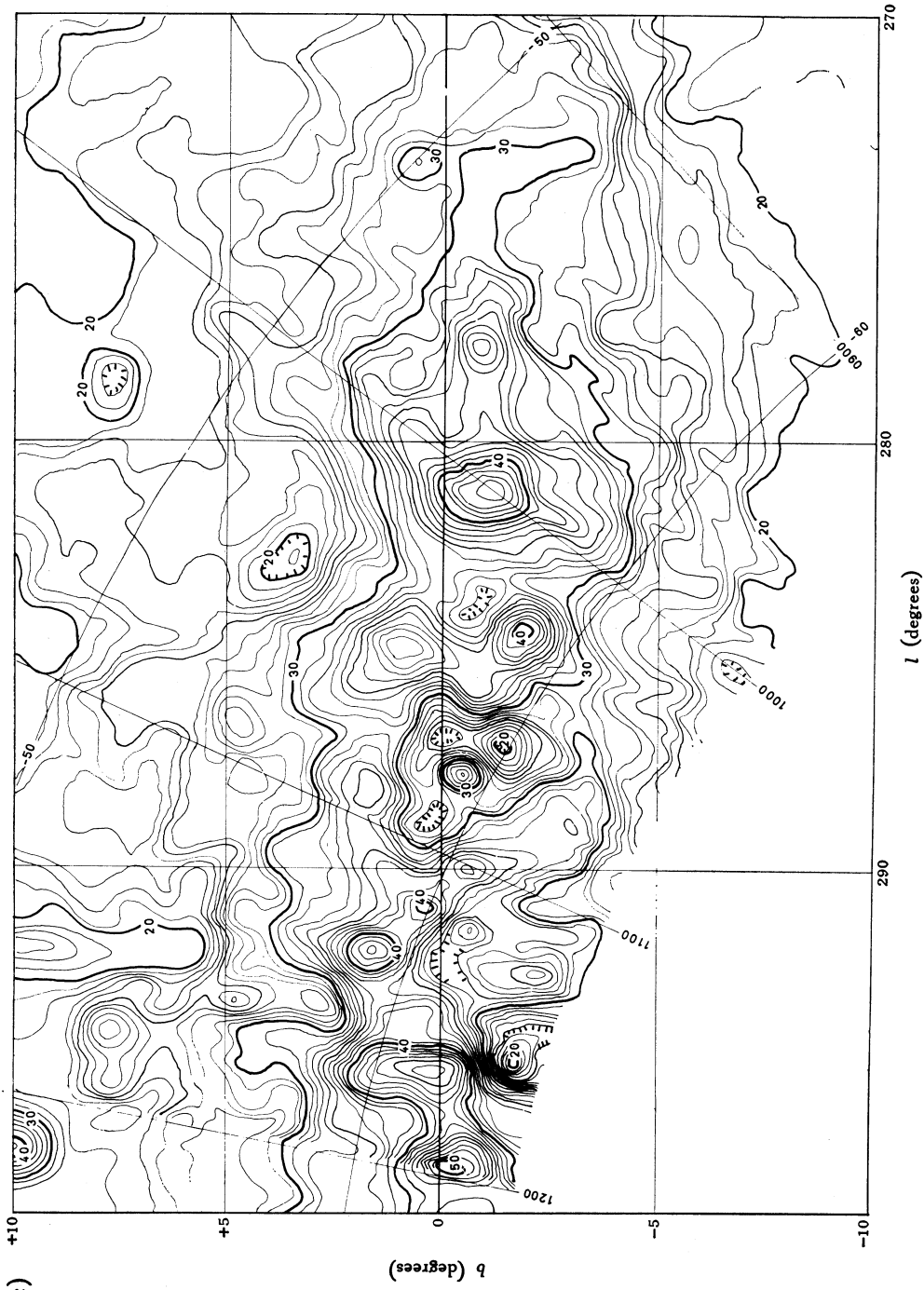
270
280
290
−10
−5
0
+5
+10
l (degrees)
b (degrees)
1200
1100
1000
0900
50
40
30
20

(2c)

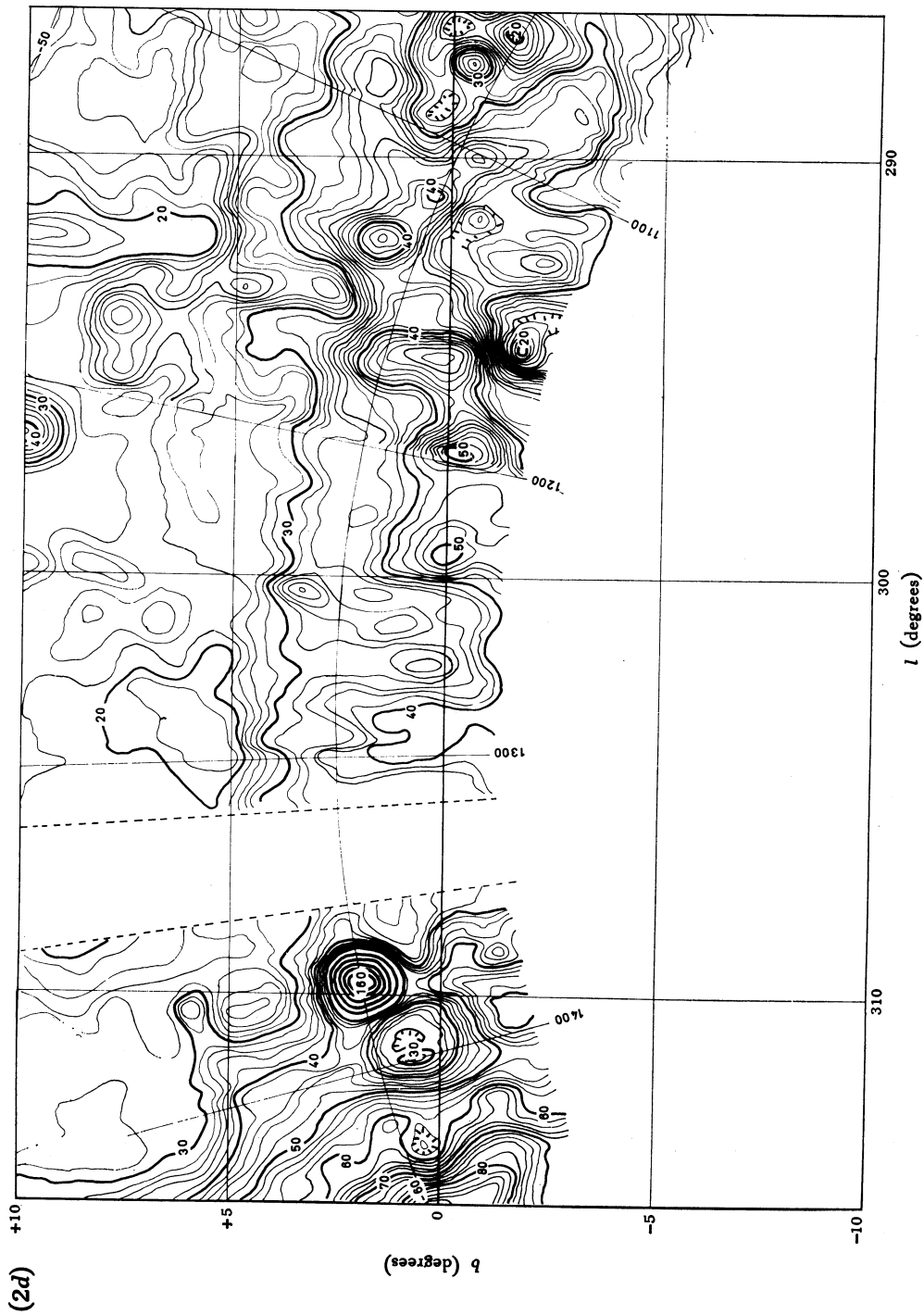

(2d)

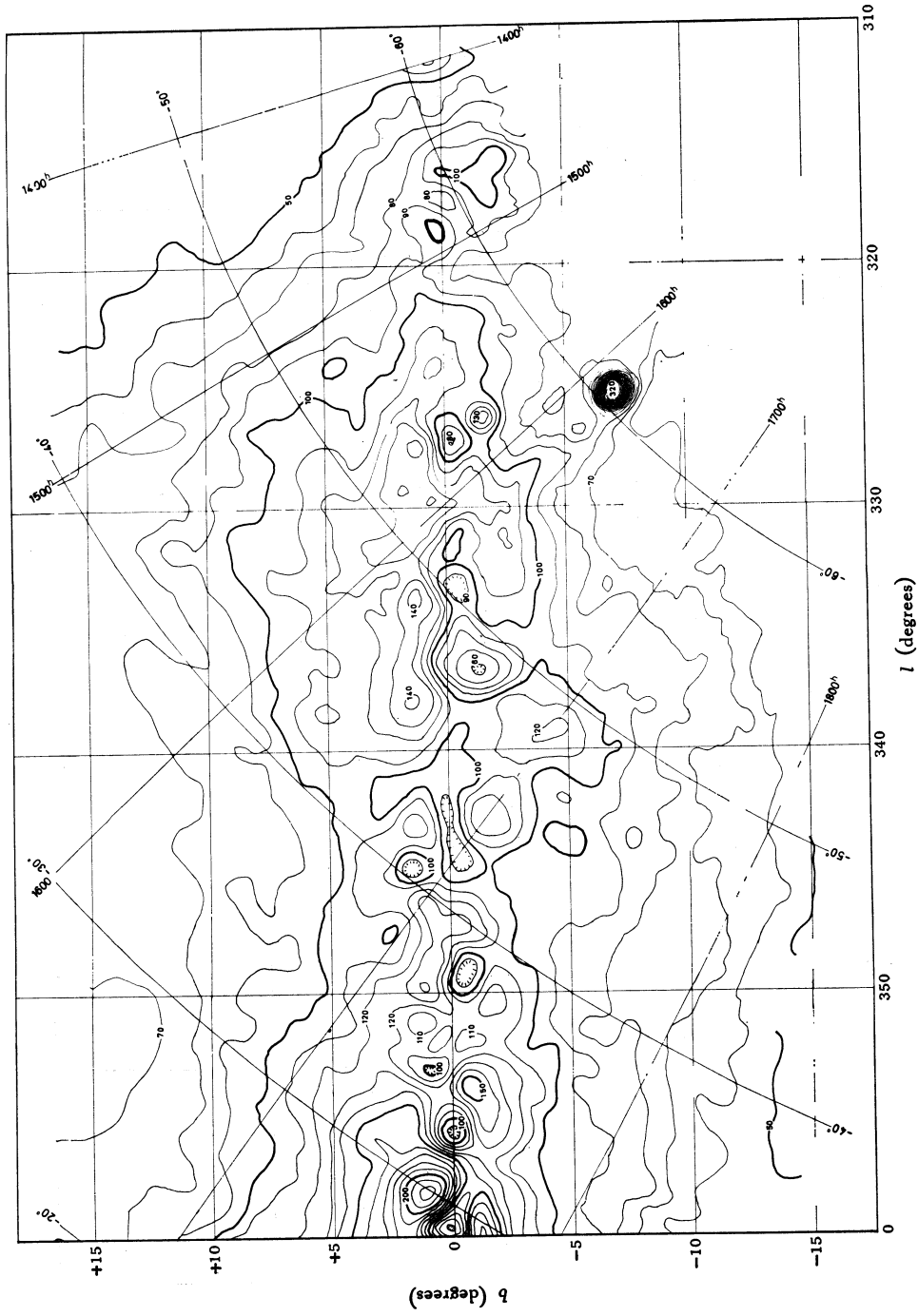
l (degrees)
b (degrees)
310
320
330
340
350
0
+15
+10
+5
0
−5
−10
−15
1400h
1500h
1600h
1700h
1800h
-60°
-50°
-40°
-30°
-20°

(2e)

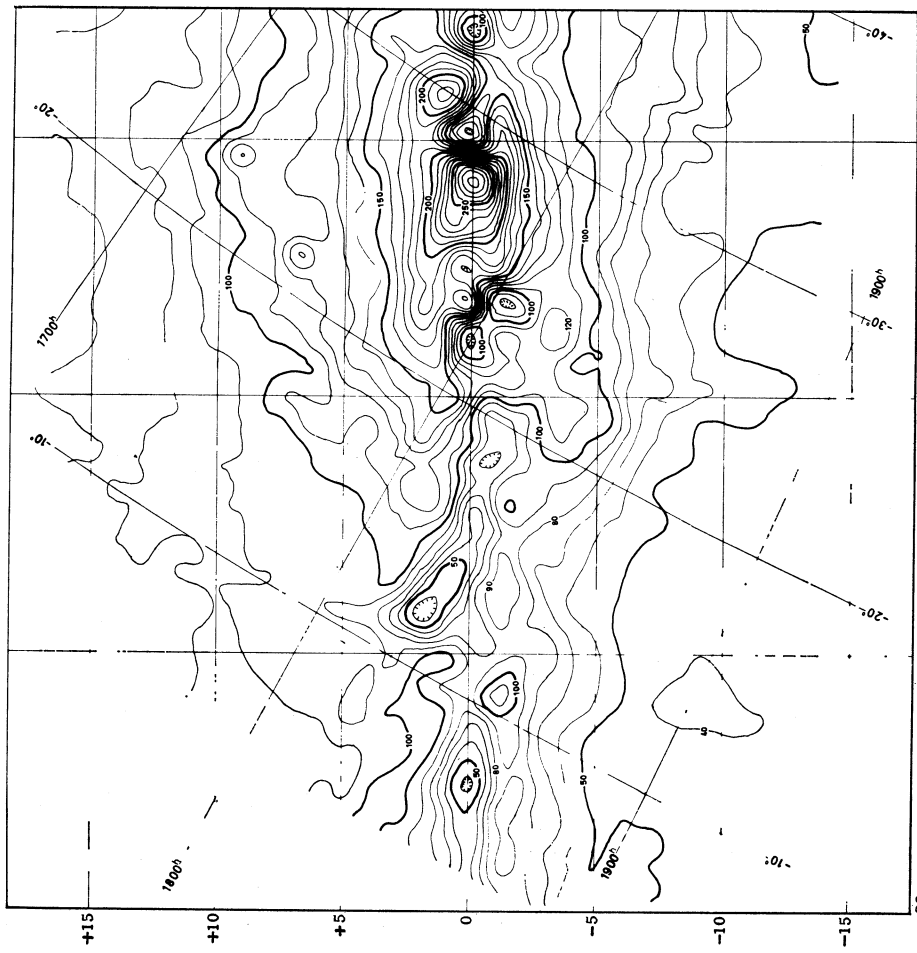

Figs 2a–2f. Survey of the galactic plane at 29·9 MHz from $l = 225°$ to 30°. A grid of 1950 celestial coordinates is superimposed on the rectangular l, b coordinates.

The high frequency map used for the comparison was that from the 1410 MHz galactic survey made with the Parkes telescope by Hill (1968). This map covers a latitude range of $\pm 3°$ and has a resolution corresponding to a beamwidth of 14′. The longitudes chosen for the comparison were ones which appeared to be free from sources at 1410 MHz over regions larger than the 29·9 MHz beam and which at

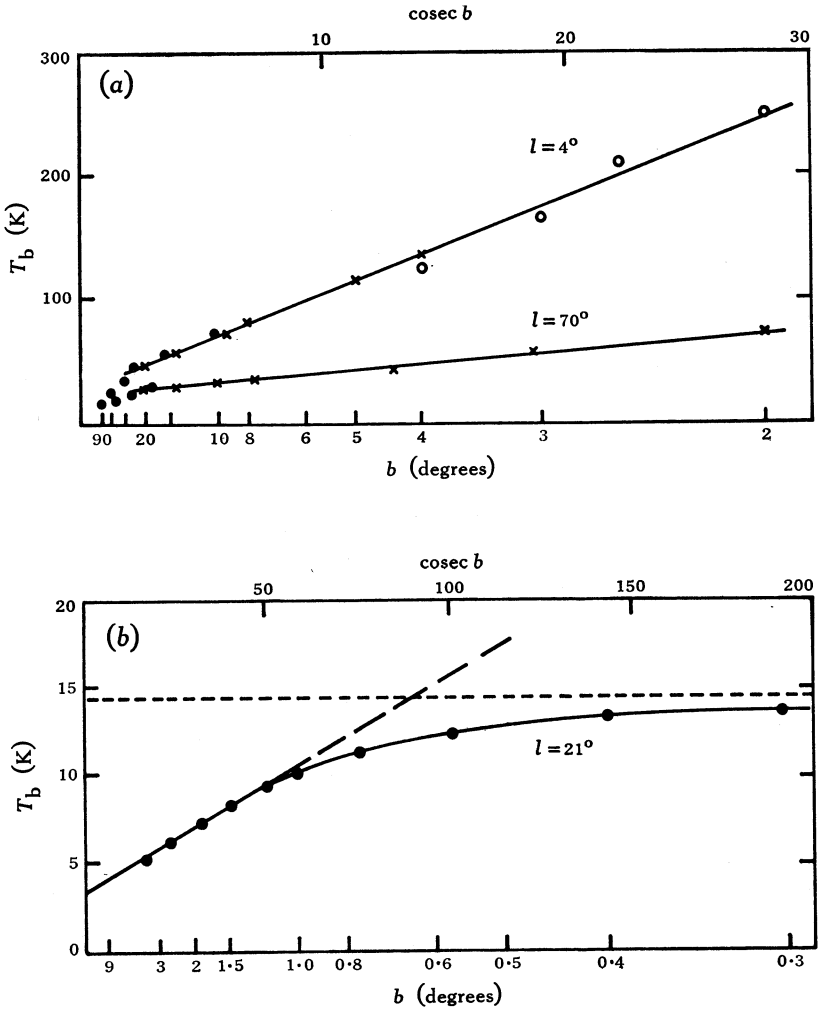

Fig. 3. Plots of T_b versus cosec b at (*a*) 400 MHz from Baldwin (1968) and (*b*) 1410 MHz from the maps of Altenhoff *et al.* (1970). The diagrams show the limits of validity $20° > |b| > 1°·3$ of the linear relation (1).

29·9 MHz did not appear to be absorbed by diffuse nearby ionized regions. Plots of T_b against cosec b for one such longitude at the two frequencies are shown in Fig. 4. At 29·9 MHz the linear relation between T_b and cosec b is followed over the range of latitudes $5° < |b| < 15°$. Within $|b| < 5°$, absorption reduces T_b relative to that given by the linear relation. The offset B is different for positive and negative values of b. This has been attributed to the slowly varying background temperature error, and

the difference between the offsets has been used to estimate a linear baseline to correct the profiles. At both frequencies the coefficients A and B in equation (1) can be found from the straight portions of the plots. Each profile can then be normalized as

$$T_n = (T_b - B)/A . \qquad (2)$$

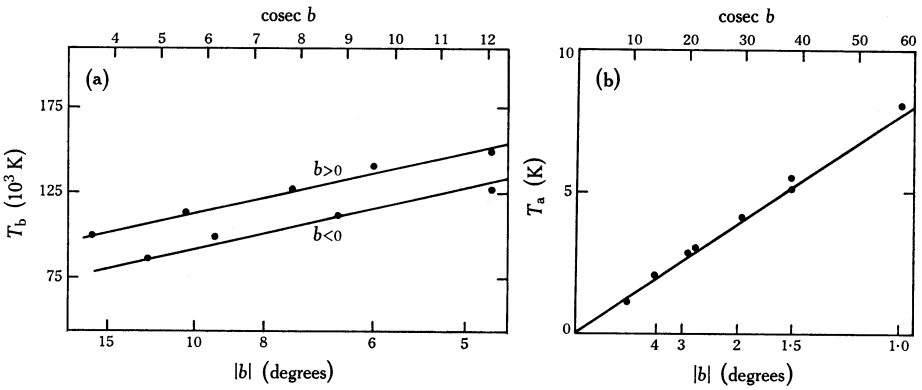

Fig. 4. Examples of plots at the same longitude $l = 347°$ of (*a*) brightness temperature T_b versus cosec b at 29·9 MHz and (*b*) antenna temperature T_a versus cosec b, prepared from the 1410 MHz map of Hill (1968). In (*a*) the displacement of the lines corresponding to the two hemispheres is probably due to incorrect restoration of the background temperature.

The optical depth of the Galaxy is very small at 1410 MHz, and the disc components of the profiles obtained at that frequency are principally due to nonthermal radiation. Since the thermal emission is concentrated towards the galactic plane with a half-width of less than 3°, it may be assumed that the portions of the 29·9 MHz profiles

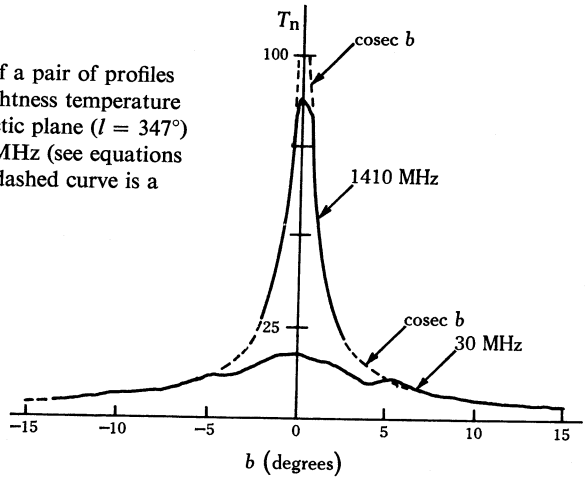

Fig. 5. Example of a pair of profiles of normalized brightness temperature T_n across the galactic plane ($l = 347°$) at 29·9 and 1410 MHz (see equations (1) and (2)). The dashed curve is a plot of cosec b.

between 5° and 15° which have a cosec b distribution are also due to nonthermal radiation, at least as far as the disc component is concerned. Hence, in the absence of thermal absorption and radiation, the T_n versus b profiles at the two frequencies should be identical. However, the central value of T_n of the 29·9 MHz profile at each longitude examined was found to be only about one-fifth of the 1410 MHz value; Fig. 5 shows one pair of these profiles. A small amount of this difference is due to the

small and rather uncertain thermal contribution which enhances the 1410 MHz peak temperature, but the main cause of the reduction of the 29·9 MHz value of T_n is thought to be interstellar ionization.

Jackson and Kerr (1971) have analysed the contour maps of Altenhoff *et al.* (1970) and estimated that, at 5 GHz, thermal emission accounts for about 30% of the continuum radiation and that the nonthermal radiation has a spectral index of −2·8. Using a spectral index of −2·1 for the thermal component and the above values, the ratio of thermal to nonthermal radiation at 1·4 GHz is 12%. The difference in beamwidth between the two surveys is of no consequence as the high optical depth at 29·9 MHz prevents the profile at that frequency from being strongly peaked at $b = 0$.

Table 1. Absorption of disc radiation

The quantities listed are: $A_{29.9}$, A_{1410}, coefficients in equation (1) for the brightness temperature; $\beta_{29.9}^{1410}$, temperature spectral index 29·9–1410 MHz; $r_{29.9}^{1410}$, ratio of scaled temperatures T_n at $b = 0$; $\tau_{29.9}$, optical depth at 29·9 MHz; E, emission measure (cm^{-6} pc); T_e, electron temperature (K); $\langle n_e^2\rangle^{\frac{1}{2}}$, r.m.s. electron density, assuming $T_e = 1000$ K and the effective length L of the absorbing region = 20 kpc

l (deg)	$A_{29.9}$ (K)	A_{1410} (K)	$\beta_{29.9}^{1410}$	$r_{29.9}^{1410}$	$\tau_{29.9}$	$E\times$ $(10^{-3}T_e)^{-1.35}$	$\langle n_e^2\rangle^{\frac{1}{2}}$ (cm^{-3})
325	6500	0·12	−2·84	0·18	5·6	470	0·15
330	8900	0·24	−2·73	0·24	4·2	350	0·13
341	9500	0·29	−2·70	0·13	7·7	660	0·18
347	6300	0·25	−2·65	0·22	4·6	390	0·14

The ratio $r_{29.9}^{1410}$ of the value of T_n at 29·9 MHz at $b = 0$ to that at 1410 MHz at $b = 0$ can be used to estimate the optical depth of the Galaxy at the chosen longitudes. If it is assumed that ionization and synchrotron emission are uniformly mixed along the line of sight, and that thermal emission may be neglected in comparison with the synchrotron emission, then

$$T_b = T_0(1-e^{-\tau})/\tau,$$

where T_0 is the brightness temperature which would be observed in the absence of absorption and τ is the optical depth. Thus an approximation to τ can be found from the relation

$$(1-e^{-\tau})/\tau = 1{\cdot}1\, r_{29.9}^{1410}.$$

Since at 29·9 MHz we have $\tau > 4$, this reduces to

$$\tau^{-1} \approx 1{\cdot}1\, r_{29.9}^{1410}.$$

(The factor 1·1 comes from the assumption that ~10% of the emission at 1410 MHz is thermal.) The optical depth of the Galaxy at 29·9 MHz has been estimated by this method at four suitable longitudes l in the range $320° < l < 350°$, giving the results listed in Table 1. There do not seem to be any other suitable values of l within 40° of the galactic centre, and at more remote longitudes the irregularity of the brightness distribution at 29·9 MHz and the poor signal to noise ratio of the 1410 MHz observations render the method unsatisfactory.

If the absorbing regions do not coincide with the emitting regions, values derived for τ will probably be overestimates. In the extreme case, if all the absorption occurred in nearby clouds, the value of τ would be about 2, rather than about 5; however, the

longitudes used were chosen to be as clear as possible of local absorbing clouds. It is to be expected that the regions of compression of the interstellar medium, where both the density of the gas and the ionizing radiation from young stars are greater, correspond to regions of enhanced magnetic field which favour the generation of synchrotron radiation. The assumption that the emitting and absorbing regions coincide, on a scale appropriate to the above determination of τ, is therefore probably reasonable.

From the relation $\tau = 8{\cdot}235 \times 10^{-2} ET_e^{-1{\cdot}35} \nu^{-2{\cdot}1}$, where E is the emission measure (cm^{-6} pc), T_e the electron temperature (K) and ν the frequency (GHz) (Mezger and Henderson 1967), the value of $ET_e^{-1{\cdot}35}$ can be derived. A value of T_e can be estimated from the ratio of thermal to nonthermal emission at 1410 MHz quoted above.

The maximum brightness temperature of 1410 MHz profiles across the galactic plane is about 20 K over the present range of longitudes, implying a thermal component of about 2 K. Thus

$$T_e \tau_{1410} \approx 2 \text{ K}$$

and, taking $\tau_{29{\cdot}9} \approx 5$ so that

$$\tau_{1410} \approx 5 \times (29{\cdot}9/1410)^{2{\cdot}1},$$

a value of $T_e \approx 1300$ K is obtained. The estimation of the thermal component of the 1410 MHz brightness is rather uncertain and so this value for T_e may easily be in error by 50%. The result obtained in this way is weighted towards low temperatures, being the value of

$$\langle \kappa T_e \rangle / \langle \kappa \rangle = \langle T_e^{-0{\cdot}35} n_e^2 \rangle / \langle n_e^2 T_e^{-1{\cdot}35} \rangle,$$

where κ is the absorption coefficient (pc^{-1}) and n_e the electron density (cm^{-3}). It is in reasonable agreement with the temperature of 1000 K deduced by Hjellming *et al.* (1969), and so we have used their figure whenever a value of T_e is required for the interpretation of our results.

Using the relation $E = \langle n_e^2 \rangle L$, where L is the effective path length through the Galaxy, and adopting values of $T_e = 1000$ K and $L = 20$ kpc, results for the r.m.s. electron density $\langle n_e^2 \rangle^{\frac{1}{2}}$ can be derived. These results are listed in Table 1.

(b) Spectral Index of Disc Emission

The factor A in equation (1) is proportional to the emissivity of the disc, and so its variation with frequency gives the temperature spectral index of the emissivity. For this purpose, the calibrations of the brightness temperature scales must be known. Values of A corresponding to $l = 347°$ have been calculated from the present work and from surveys at 85·7 MHz (Hill *et al.* 1958), 150 MHz (Landecker and Wielebinski 1970), 408 MHz (Komesaroff 1966) and 1410 MHz (Hill 1968), and Fig. 6 shows them plotted against frequency. A good fit to a straight line is obtained if the 85·7 MHz point is disregarded, yielding a value of $-2{\cdot}72$ for the spectral index. This value refers only to the disc radiation and is unaffected by whatever isotropic component is present, or by errors in the zero levels of the maps. Values of the spectral index which are based only on the 29·9 and 1410 MHz values of A are given in Table 1 for four longitudes in the range $320° < l < 350°$ (including $l = 347°$). They are not very different from the value derived from Fig. 6.

The galactic survey map of Hill (1968) is drawn in contours of antenna temperature rather than full beam brightness temperature and so a conversion factor was calculated from the following data: the calibration source 13S6A, which has a strength of 108 Jy at 1410 MHz (Manchester 1969), produced an increment of 53 K in antenna temperature, and the full beam solid angle of the Parkes telescope was $1{\cdot}83 \times 10^{-5}$ sr (Beard 1966). From these values it appears that 1 K antenna temperature equals 1·79 K brightness temperature.

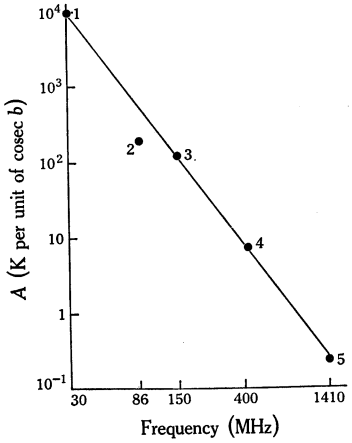

Fig. 6. Plot of the coefficient A of cosec b in equation (1) versus frequency at $l = 347°$. The data used to calculate the values of A are from:

1. Present work
2. Hill *et al.* (1958)
3. Landecker and Wielebinski (1970)
4. Komesaroff (1966)
5. Hill (1968)

An indication of the average disc emissivity at 29·9 MHz may be obtained from the deduced 29·9 MHz temperature due to the disc component at $b = 0°$ in directions close to $l = 0°$. This is the brightness temperature which would be measured in the absence of absorption and equals:

$$0{\cdot}9\, A_{30}\, T_{\max}^{1410} / A_{1410},$$

in the notation of the previous subsection. At $l = 347°$ this has a value of 610 000 K. If a path length of 20 kpc is assumed the average emissivity at 29·9 MHz is 30 K pc^{-1}.

4. Discrete Absorption Regions

Very close correlation is found between the regions of depressed brightness at 29·9 MHz (indicated on the maps by cross hatching of the innermost contour) and optically observed emission nebulae. Typically, an optical depth of unity at 30 MHz corresponds to an emission measure of about 1500 cm^{-6} pc for values of T_e in the vicinity of 8000 K. The optical depth is approximately proportional to the Hα line intensity, the ratio being only weakly dependent on temperature. The line intensity for $\tau_{30} = 1$ corresponds to regions described as 'very faint' in the Hα catalogue of southern sources compiled by Rodgers *et al.* (1960; RCW catalogue). In order that an HII region should be detected as a 30 MHz absorption region it must have $\tau \gtrsim 1$, have an angular extent of the order of one beamwidth and be sufficiently close that the ratio of background to foreground nonthermal emission is large. All these conditions favour the detection of large relatively diffuse nearby nebulae which are likely to be observed optically.

Table 2 gives a list of the discrete absorption regions observed at 29·9 MHz. The entries in the table are:

Column 1. Galactic coordinates of the centre of the region measured at 29·9 MHz.

Column 2. Dimensions in l and b directions measured at 29·9 MHz.

Column 3. Identification with nebula listed in the RCW catalogue. The criterion for these identifications was that the position given by RCW lay within the absorbing region and that the angular size of the nebula quoted by RCW was larger than one-quarter of the 29·9 MHz beam area. Parentheses indicate that the identification is uncertain.

Column 4. Dimensions quoted in the RCW catalogue.

Column 5. Fractional reduction in the brightness temperature $\Delta T_b/T_b$.

Column 6. Minimum temperature in the depression T_{min}.

Column 7. Distance, derived from: GG, Georgelin and Georgelin (1970), photometric unless otherwise noted; W, Wilson *et al.* (1970), recombination line kinematic; TV, Thé and Vleeming (1971), photometric.

Table 2. Discrete absorption regions at 29·9 MHz

(1) Position l°	b°	(2) Angular size Δl°	Δb°	(3) RCW No.	(4) Optical size (min arc)	(5) Reduction $\Delta T_b/T_b$	(6) T_{min} (10^3K)	(7) Distance (kpc)		(8) Notes[A]
224·3	−1·2	1·5	1	1	150×150	0·04	34	0·8	GG	1
236·3	−6·6	5	3	15	300×300	0·33	17			
248·3	−0·4	1	1			0·17	20			
251·0	−1·5	2	1·5			0·21	22			
255·9	−0·9	2	1			0·11	33			
260·4	+0·8	1·5	1·5	27	100×100	0·08	35			
261·8	−10·0	1	4			0·22	20			
268·7	−1·7	2	3	38, 40	40×40	0·20	29	0·6	W	2
283·9	−0·6	1·5	2	47, 48, 49		0·06	44	3·6	GG	3
287·5	−0·5	3	3	53, 54		0·35	29	2·5	TV	4
291·5	−0·6	1	1	57	170×40	0·12	42	3·5	GG	
294·4	−1·7	2	2	60, 61, 62		0·35	43	1·8	GG	5
293·2	+2·7	1	3	59	180×150	0·18	42	2·9	GG	6
293·2	+4·7					0·11	34			
320·0	−1·8	1·5	2·5	(89)		0·13	84	1·0	GG	7
327·1	−0·3	2	1·5	97, 98		0·32	87	3·4	GG	
333·2	−0·4	1	1	106	35×20	0·16	124	1·9	GG	
336·7	−1·3	2	3	108	210×120	0·56	58	1·3	GG	8
342·1	+0·0	5	4	113	360×300	0·28	105	2·0	GG	
344·4	−0·4									
344·9	+1·6	1·5	1·5	119	180×145	0·30	100	1·6	GG	3
349·1	−0·6	1·5	1	123	75×75	0·32	100	2·0±1·5	W	
353·2	+0·9	0·5	0·5	131	170×55	0·20	115	1·6	GG	
355·6	+0·0	0·8	0·8	132	110×80	0·36	98	1·4	GG	
359·6	+0·1	1·5	1·0	(134, 137)		0·44	127			
6·3	−1·4	0·8	1·5	146	120×90	0·43	92	1·6	GG	9
7·8	+0·0	1	0·8			0·27	110			
12·4	−0·9	2·5	1	151 (153)	100×35	0·3	98	2·6	GG	
18·4	+1·7	2·5	2	167	180×90	~0·6	60	2·3	GG	
25·4	+0·0	3	1·5				62			10

[A] Notes:

1. NGC2327.
2. RCW 38 size in column 4.
3. Kinematic distance in column 7.
4. Carina nebula, optically deep over beamwidth.
5. λ Centauri nebula.
6. Extended, two main depressions.
7. Extended high frequency emission region.
8. Optically deep over beamwidth.
9. M8.
10. Complex region, many thermal sources in Altenhoff *et al.* (1970).

Table 3. Nonthermal sources detected at 29·9 MHz

(1) Position l °	b °	(2) Position (1950) R.A. h m	Dec. °	(3) MSH source No.[A]	(4) Angular size[B] Δl°	Δb°	(5) Flux[C] $S_{29\cdot9}$ (Jy)	(6) Estimated $\Delta S_{29\cdot9}$ (Jy)	(7) Other identifications and notes[D]
221·8	+0·1	07 05·7	−7·8				47	±7	PKS 0705−07, extragalactic
225·4	+3·0	07 22·9	−9·6	07−*04*			41	17	PKS, CUL 0722−09, S gal, absorbed by RCW 4
226·2	+6·8	07 37·9	−8·4				40	20	
233·9	−5·0	07 10·2	−20·8	07−*23*			46	7	PKS, CUL 0709−20, extragalactic
235·6	−9·3	06 56·8	−24·3	06−*216*			75	8	PKS, CUL 0656−24, extragalactic, absorbed by extension of RCW 15
236·2	+3·1	07 45·0	−18·9	07−*117*			76	8	PKS, CUL 0745−19, D gal.
238·3	−5·9	07 15·5	−25·1	07−*24*			32	12	PKS 0715−25, CUL 0715−24, extragalactic, possibly absorbed by RCW 15
240·8	−1·2	07 39·0	−25·1	(07−*212*)	1·2	1·2	40	12	SNR?
241·6	−9·3	07 08·5	−29·6	07−*22*			35	12	
242·5	−3·5	07 33·8	−27·7		1·0	1·0	38	12	
248·8	−4·1	07 45·9	−33·4		2·9	2·0	75	12	SNR?
249·6	+4·0	08 20·0	−29·7	08−*23*			52	7	PKS 0819−30, E gal.
251·9	−8·1	07 36·2	−38·1	07−*312*			32	6	CUL 0736−38, extragalactic
253·9	−6·0	07 50·5	−38·8				31	10	
255·7	+0·4	08 22·7	−36·8		1·5	1·0	38	14	SNR?
256·0	−3·3	08 08·0	−39·1	08−*31*			53	18	PKS, CUL 0807−38, extragalactic
260·4	−3·3	08 21·1	−42·8	08−*44*	0·7	0·7	1050	60	Puppis A, SNR, Milne 13
261·9	+5·5	09 02·3	−38·5	09−*32*	0·5	0·5	42	17	PKS 0902−38, SNR, Milne 14
262·7	−0·6	08 40·4	−43·0						
263·9	−2·9	08 34·3	−45·4	08−*45*	6·5	6·5			Peaks of Vela SNR, Milne 15, *see note 1*
265·4	−1·0	08 48·1	−45·3						
274·8	+0·6	09 34·1	−51·0				32	12	
277·8	−0·9	09 42·5	−54·1		0·8	0·8	46	10	SNR?
281·2	−1·0	10 00·8	−56·3	(10−*51*)	1·5	1·5	200	25	SNR? *see note 2*
284·4	−1·8	10 17·0	−58·8	10−*53*			70	12	SNR, Milne 16, partly absorbed
284·8	+1·0	10 30·6	−56·6		1·5	1·5	47	16	SNR?
287·8	−0·4	10 45·4	−59·3				81	8	SNR, *see note 3*

290·0	−0·7	11	00·2	−60·5	11−*61*			35	7	SNR, Milne 19, partly absorbed
292·0	+1·6	11	21·7	−59·1	11−*54*			58	15	SNR, Milne 21
293·9	+7·8	11	47·6	−53·7	(11−*56*)			39	10	
296·7	+10·0	12	08·5	−52·1	12−*51*	1·5	1·5	200	24	SNR, RCW 63
296·8	−0·3	11	55·3	−62·3				93	20	SNR, *see note 4*
309·7	+1·8	13	43·1	−60·1	13−*62*			1680	118	13S6A, SNR?, Milne 28, 29
316·1	+0·0	14	36·3	−59·9	14−*57*			80	30	SNR, Milne 32, partly absorbed
324·3	+0·4	15	28·5	−55·5	15−*54*	1·0	1·0	90	30	SNR?
325·3	−7·1	16	10·1	−60·7	16−*61*			3190	220	PKS 1610−60·8, 1610−60·5, 16S6A, E gal.
326·5	−1·6	15	49·4	−55·8	15−*56*			371	42	SNR, Milne 36
331·7	+11·3	15	27·3	−42·3	15−*43*			175	14	CUL 1526−42, extragalactic
333·8	+1·4	16	12·4	−48·7		1·0	1·0	125	35	
338·0	+1·5	16	29·4	−45·6				134	35	
358·1	+1·1	17	33·5	−29·9		1·5	1·0	460	100	Part of galactic nucleus complex
0·7	+9·2	17	10·2	−23·3	17−*23*			215	16	Extragalactic
1·6	+0·0	17	46·2	−27·6		2·0	2·0	500	100	Part of galactic nucleus complex
4·6	+6·8	17	27·9	−21·4	17−*211*			276	20	Kepler's nova, SNR, PKS, CUL 1727−21
6·3	+0·3	17	55·7	−23·4	17−*216*			157	16	SNR, Milne 57, partly obscured
21·8	−0·6	18	30·3	−10·2		1·0	1·0	210	40	

[A] Parentheses indicate poor agreement of positions.

[B] Angular size at 29·9 MHz in l and b directions. No entry indicates that the source is not appreciably resolved. The values were obtained from the contour maps and are included only as a rough guide.

[C] This is the peak flux density if there is no entry in column 4; otherwise it is the integrated flux density calculated from six sections through the source.

[D] Other identifications are from: revised PKS catalogue (Ekers 1969); CUL catalogue (Slee and Higgins 1973); Milne (1970). Additional notes are:

1. G262·7−0·6 to G265·4−1·0. The emission from the Vela supernova remnant extends over a greater region at 30 MHz than at high frequencies. A region of high emission extends to $l = 258°$, $b = -7°$. No flux integration has been carried out because of the difficulty in deciding the limits of the source.
2. G281·2−1·0. This extended source is probably a supernova remnant and may be associated with the nearby pulsar MP 0959.
3. G287·8−0·4. This is a supernova remnant in front of the Carina nebula (Jones 1973).
4. G296·8−0·3. This is the Crux supernova remnant, associated with the pulsar PSR 1154−62 (Large and Vaughan 1972).

All the observed absorption regions are at distances of less than 4 kpc, presumably due to the fact that foreground emission reduces the depression produced by distant HII regions, and this fact permits a decision between the near and far kinematic distances of radio HII regions in some cases. The HII complex shown on the 1410 MHz map of Hill (1968) extending over $315°{\cdot}5 < l < 318°$ and $-0°{\cdot}7 < b < 1°{\cdot}0$ does not appear as an absorption region at 29·9 MHz. The two kinematic distances determined from H109α line measurements are 3 and 12 kpc (Shaver and Goss 1970*b*), and 12 kpc is therefore the correct one. The detection of the complex surrounding G343·5−0·0 and G342·5+0·2 indicates that the near distance (3·2 kpc) is applicable rather than the far distance (16·0 kpc).

If an HII region is optically deep over an area larger than a beamwidth, the emissivity of the Galaxy along the line of sight to the nebula can be obtained from the excess of the apparent brightness temperature of the nebula over its electron temperature. Since only nearby HII regions have been detected at 29·9 MHz, this method is limited to finding the emissivity within a few kiloparsecs of the Sun. Only two HII regions appear to be optically deep over the whole beamwidth, namely the Carina nebula and RCW 108. The emissivities $J_{29·9}$ derived using these nebulae are set out below.

	l	Distance	$T_{min}-T_e$	$J_{29·9}$
Carina nebula	287°	2·5 kpc	23 000 K	9·2 K pc^{-1}
RCW 108	337°	1·3 kpc	49 000 K	38 K pc^{-1}

5. Nonthermal Sources

All the nonthermal sources which have been detected at 29·9 MHz within the region covered by the maps (Figs 2*a*–2*f*) are listed in Table 3 together with information on their size and flux density. Apart from a few extragalactic sources, the list consists of known supernova remnants and a number of extended objects of low surface brightness, probably supernova remnants (because they are confined to within a few degrees of the plane) which have not previously been reported. The present instrument is well suited to detect such objects although, at longitudes less than about 50° from the galactic centre, absorption by HII regions and interstellar ionized gas obscures a number of sources seen at higher frequency, and confusion due to the variations in brightness between the intense disc radiation and absorption regions prevents the recognition of weaker sources in this range of longitudes.

The positions of the sources in Table 3 were measured from the 29·9 MHz contour maps in galactic coordinates and rounded to 0°·1. The 1950·0 right ascensions and declinations are also listed. To assess the accuracy of the positions obtained from the 29·9 MHz maps, the positions of 50 point sources away from the galactic plane were measured and compared with the positions given in the Parkes catalogue. The r.m.s. difference was 0°·13 with no apparent systematic error or systematic dependence on zenith angle. In three cases the error was 0°·3, which was the maximum. Details of a number of the unresolved sources listed in Table 3 have been reported by Finlay and Jones (1973).

A number of undetected sources which have nonthermal spectra and extrapolated 29·9 MHz flux densities large enough to have allowed their detection are listed in Table 4. In several cases the classification of the source as nonthermal is probably mistaken, but in most cases absorption must account for the failure to observe them

at 29·9 MHz. Many of the sources listed in Table 4 lie within depressions in the background radiation. It seems likely that the HII responsible for the depression in the background level is at least partly responsible for the absorption of the discrete sources. It is interesting to note that Sagittarius A, the nonthermal source in the galactic nucleus, appears as though obscured by the relatively nearby HII region which obscures the background between $l, b = 0°{\cdot}2, +0°{\cdot}0$ and $359°{\cdot}0, -0°{\cdot}5$.

At the outset it was hoped that values of optical depth τ for lines of sight of known length could be obtained from the low-frequency deficiencies of spectra of discrete nonthermal sources. However, of the six sources which showed absorption at low frequencies (PKS 0656−24, 0722−09 and MSH 10−*53*, 11−*61*, 14−57, 17−*216*), all but one, MSH 14−57, were rejected on various grounds. Using the higher frequency flux densities of Mills *et al.* (1961), Day *et al.* (1969) and Shaver and Goss (1970*a*), a value of $\tau = 1{\cdot}3 \pm 30\%$ was obtained for the interstellar medium between the Sun and this source. Since Shaver and Goss (1970*b*) give a distance of 4·2 kpc for the source, this result is not inconsistent with the value of $\tau = 5{\cdot}6$ given in Table 1 for a path right through the Galaxy at $l = 325°$.

Table 4. Nonthermal sources not detected at 29·9 MHz

Galactic source No.[A]	Milne catalogue No.	MSH source No.	Extrapolated $S_{29{\cdot}9}$ (Jy)[B]	Upper limit to $S_{29{\cdot}9}$ (Jy)
289·1−0·4	17		220	30
291·0−0·1	20	11–*62*	330	30
320·4−1·0	33	15–*52*	280	30
327·4+0·4	37		415	35
328·4+0·2	39	15–*57*	215	35
332·5+0·1	42	16–*51*	>256	50
332·4−0·4	43		70	50
337·0−0·1	45		525	60
342·1+0·1	48	16–*48*	300	60
348·5+0·1	49, 50	17–*33*	730	70
349·7+0·2	51		186	70
355·2+0·1	52		244	70
357·7−0·1	53		310	70
5·3−1·1	56		106	70
18·9+0·3	59	18–*18*	250	70
21·8−0·5	60	18–*113*	770	60

[A] Coordinates from Milne (1970).
[B] Value at 29·9 MHz from extrapolation of flux densities given by Milne (1970).

6. Summary of Results and Discussion

Absorption by galactic disc. The optical depth τ of the Galaxy in the galactic plane has been estimated in four directions within the range $320° < l < 350°$ by a method which does not depend on the absolute brightness temperature calibration of the 29·9 MHz synthesis telescope. The values of τ obtained lie between 4·2 and 7·7. It does not seem possible to obtain much information from the 29·9 MHz results about absorption along paths at longitudes remote from the galactic centre, but the mean absorption coefficient in these directions is certainly lower than in directions close to the centre. Comparison of absolute temperatures from the 29·9 MHz maps and the 150 MHz maps of Landecker and Wielebinski (1970) indicate that for $l < 250°$

the optical depth is less than 0·5 and the failure of the source PKS 0705–07, which lies close to the plane, to show absorption at 29·9 MHz suggests an even lower limiting value.

Electron temperature of interstellar medium. By combining the above values of τ with high frequency data, an estimate has been found for the electron temperature of the interstellar medium, exclusive of nearby HII regions, which is consistent with the value of 1000 K suggested by Hjellming *et al.* (1969) for the hot component of their proposed galactic model.

R.M.S. electron density. Taking the values of τ in Table 1, the quantity $\langle n_e^2 \rangle^{\frac{1}{2}}$ has been estimated for paths through the Galaxy in the region $320° < l < 350°$ using a path length of 20 kpc and an electron temperature of 1000 K. The resulting values lie between 0·13 and 0·18 cm^{-3}. Of the methods used by other workers to obtain estimates of $\langle n_e^2 \rangle^{\frac{1}{2}}$, those which apply most nearly to the same region of the Galaxy are the H109α line measurements of Jackson and Kerr (1971) and the H157α line measurements of Gordon and Gottesman (1971), both of which give values in the range 0·15–0·3. Most of the line emission reported by these workers is thought to have originated in the Sagittarius and Norma–Scutum arms (Jackson and Kerr). Values obtained by Dulk and Slee (1972) from the absorption of supernova remnants at 80 MHz were a little higher, being within the range 0·15–0·5 cm^{-3}, again assuming an electron temperature of 1000 K. Several of the supernovae used for their work lie in regions in which the background radiation is absorbed strongly at 29·9 MHz and the absorption along these paths may not be representative. Finally, pulsar dispersion measurements suggest values of $\langle n_e \rangle$ of the order of 0·06 cm^{-3} over paths up to about 4 kpc from the Sun (Mills 1970) and 0·1 cm^{-3} in the local arm (Gould 1971). These values agree fairly well with the above estimates of $\langle n_e^2 \rangle^{\frac{1}{2}}$, suggesting a fairly uniform electron density.

Nonthermal galactic emission. The temperature spectral index of the nonthermal emissivity of the galactic disc in the direction $l = 347°$ has been found in Section 3*b* to be $-2·72$ between 1410 and 29·9 MHz. An average value of the nonthermal emissivity of the disc in the same direction has been deduced as 30 $\mathrm{K\,pc}^{-1}$. It has also been possible to estimate the average emissivity along paths to two optically dense HII regions from their apparent brightnesses. The values obtained were 38 $\mathrm{K\,pc}^{-1}$ in the direction of RCW 108 ($l = 337°$) and 9·2 $\mathrm{K\,pc}^{-1}$ in the direction of the Carina nebula ($l = 287°$). The low value in the latter case suggests that an interarm gap may separate the Sun from the Carina nebula (Jones 1973).

Discrete absorption regions. About 29 absorption regions have been identified with optically observed HII regions (see Section 4). Only nearby regions are observed, and this fact permits a choice between ambiguous kinematic distances in two cases.

Nonthermal sources. A number of previously unlisted nonthermal sources have been observed. Many of these are objects of low surface brightness and probably are supernova remnants because of their concentration towards the galactic plane.

References

Altenhoff, W. J., Downes, D., Goad, L., Maxwell, A., and Rinehart, R. (1970). *Astron. Astrophys. Suppl. Ser.* **1**, 319.

Baldwin, J. E. (1968). Proc. I.A.U. Symp. No. 31, p. 337 (Reidel: Dordrecht, Holland).

Beard, M. (1966). *Aust. J. Phys.* **19**, 141.

Day, G. A., Thomas, B. M., and Goss, W. M. (1969). *Aust. J. Phys. Astrophys. Suppl.* No. 11, 11.

Dulk, G. A., and Slee, O. B. (1972). *Aust. J. Phys.* **25**, 429.
Ekers, J. A. (1969). *Aust. J. Phys. Astrophys. Suppl.* No. 7.
Finlay, E. A., and Jones, B. B. (1972). *Proc. Astron. Soc. Aust.* **2**, 115.
Finlay, E. A., and Jones, B. B. (1973). *Aust. J. Phys.* **26**, 389.
Georgelin, Y. P., and Georgelin, Y. M. (1970). *Astron. Astrophys.* **6**, 349.
Gordon, M. A., and Gottesman, S. T. (1971). *Astrophys. J.* **168**, 361.
Gould, R. J. (1971). *Astrophys. Space Sci.* **10**, 265.
Hill, E. R. (1968). *Aust. J. Phys.* **21**, 735.
Hill, E. R., Slee, O. B., and Mills, B. Y. (1958). *Aust. J. Phys.* **11**, 530.
Hjellming, R. M., Gordon, C. P., and Gordon, K. J. (1969). *Astron. Astrophys.* **2**, 202.
Jackson, P. D., and Kerr, F. J. (1971). *Astrophys. J.* **168**, 29.
Jones, B. B. (1973). *Aust. J. Phys.* **26**, 545.
Komesaroff, M. M. (1966). *Aust. J. Phys.* **19**, 75.
Landecker, T. L., and Wielebinski, R. (1970). *Aust. J. Phys. Astrophys. Suppl.* No. 16.
Large, M. I., and Vaughan, A. E. (1972). *Nature (London) Phys. Sci.* **236**, 117.
Manchester, B. A. (1969). *Aust. J. Phys. Astrophys. Suppl.* No. 12.
Mathewson, D. S., Broten, N. W., and Cole, D. J. (1965). *Aust. J. Phys.* **18**, 665.
Mezger, P. G., and Henderson, A. P. (1967). *Astrophys. J.* **147**, 471.
Mills, B. Y. (1970). Proc. I.A.U. Symp. No. 38, p. 178 (Reidel: Dordrecht, Holland).
Mills, B. Y., Slee, O. B., and Hill, E. R. (1961). *Aust. J. Phys.* **14**, 497.
Milne, D. K. (1970). *Aust. J. Phys.* **23**, 425.
Rodgers, A. W., Campbell, C. T., and Whiteoak, J. B. (1960). *Mon. Notic. Roy. Astron. Soc.* **121**, 103.
Shaver, P. A., and Goss, W. M. (1970*a*). *Aust. J. Phys. Astrophys. Suppl.* No. 14, 77.
Shaver, P. A., and Goss, W. M. (1970*b*). *Aust. J. Phys. Astrophys. Suppl.* No. 14, 133.
Slee, O. B., and Higgins, C. S. (1973). *Aust. J. Phys. Astrophys. Suppl.* No. 27.
Thé, P. S., and Vleeming, G. (1971). *Astron. Astrophys.* **14**, 120.
Wilson, T. L., Mezger, P. G., Gardner, F. F., and Milne, D. K. (1970). *Astron. Astrophys.* **6**, 364.

Manuscript received 25 March 1974